Gondwana Research 94 (2021) 1–11

Contents lists available at ScienceDirect

Gondwana Research

journal homepage: www.elsevier.com/locate/gr

Oldest-known Neoproterozoic carbon isotope excursion: Earlier onset of Neoproterozoic carbon cycle volatility

Zhiyue Zhang [a,b,c], Peng Peng [a,b,c,*], Lianjun Feng [b,c,d], Zheng Gong [e], Ross N. Mitchell [a,c,*], Youlian Li [a,c]

[a] State Key Laboratory of Lithospheric Evolution, Institute of Geology and Geophysics, Chinese Academy of Sciences, Beijing 100029, China
[b] College of Earth and Planetary Sciences, University of Chinese Academy of Sciences, Beijing 100049, China
[c] China-Brazil Joint Research Center, Innovation Academy for Earth Science, Chinese Academy of Sciences, Beijing 100029, China
[d] Key Laboratory of Mineral Resources, Institute of Geology and Geophysics, Chinese Academy of Sciences, Beijing 100049, China
[e] Department of Earth and Planetary Sciences, Yale University, 210 Whitney Avenue, New Haven, CT 06511, USA

ARTICLE INFO

Article history:
Received 10 November 2020
Received in revised form 5 January 2021
Accepted 6 January 2021
Available online 16 February 2021

Keywords:
North China Craton
Neoproterozoic
Dalian basin
Carbon isotopes
Paleogeography

ABSTRACT

The Neoproterozoic Era (1000–541 Ma) is characterized by the largest negative carbon isotope excursions in Earth history. Younger Neoproterozoic excursions are well-documented on multiple continental margins and associated with major events including snowball Earth glaciations, ocean-atmosphere oxygenation, and the evolution of animal multicellularity. However, due to a large gap in carbon isotopes before 900 Ma, the onset of early Neoproterozoic carbon cycle volatility has heretofore been obscure. Here, we present a mid-amplitude, negative carbon isotope excursion with $\delta^{13}C$ values reaching a nadir of ~ − 6‰ from the Majiatun Formation in the Dalian Basin of the North China Craton dated between 950 and 920 Ma. The whole-rock $^{87}Sr/^{86}Sr$ ratios of limestone and dolostone are as low as ~0.7055, which is compatible with the Tonian age of the global carbonate curve. Identification of the Majiatun anomaly thus fills the critical gap in carbon isotopes and implies the onset of Neoproterozoic carbon cycle volatility ~130 m.y. earlier than previously thought. Now 5 negative carbon isotope excursions occur with increasing amplitude throughout Neoproterozoic time, implying deeper roots for the biogeochemical processes that may have causally led to late Neoproterozoic snowball glaciation, oxygenation, and biological innovation.

1. Introduction

The Neoproterozoic Era (1000–541 Ma) is one of the most dynamic intervals of global change in Earth history, with large and episodic perturbations to the carbon cycle (Cox et al., 2016), severe snowball Earth glaciations (Hoffman et al., 2017), and the rise of atmospheric oxygen and large Metazoa (Lyons et al., 2014). The Neoproterozoic carbon isotope excursions are the most negative anomalies recorded in Earth history (Grotzinger et al., 2011; Rose et al., 2012) and are intimately linked with the notable events occurring in the cryosphere, ocean-atmosphere, and biosphere at this time. Practically, the isotopic anomalies diagnostic of the era are also one of the chief ways that Neoproterozoic stratigraphic sequences in basins of different continental margins are correlated (Cox et al., 2016). Establishing a complete Neoproterozoic carbon isotope record would thus benefit stratigraphic correlations as well as efforts to better understand the roots of the late Neoproterozoic dramatic environmental changes. Defining exactly when in early Neoproterozoic time the start of carbon isotope fluctuations began is thus critical in order to establish the temporal origins of early Neoproterozoic biogeochemical processes that preceded the profound late Neoproterozoic environmental changes.

Here we focus on the carbon isotope chemostratigraphy of earliest Neoproterozoic time (the Tonian Period, 1000–720 Ma). An accurate understanding of marine carbon biogeochemical cycles and global correlations of Tonian strata is difficult due to both generally limited stratigraphic preservation and age constraints. In the Tonian $\delta^{13}C$ compilation, there are few records between 1000 and 900 Ma (Cox et al., 2016). Thus, except for the well-constrained ca. 811 Ma Bitter Springs anomaly (Maloof et al., 2006) and the ca. 735 Ma Islay anomaly (Macdonald et al., 2010) during the later Tonian, any indication of putative $\delta^{13}C$ excursions with reliable early Tonian age constraints is lacking.

* Corresponding authors at: State Key Laboratory of Lithospheric Evolution, Institute of Geology and Geophysics, Chinese Academy of Sciences, Beijing 100029, China.
E-mail addresses: pengpengwj@mail.iggcas.ac.cn (P. Peng), ross.mitchell@mail.iggcas.ac.cn (R.N. Mitchell).

https://doi.org/10.1016/j.gr.2021.01.013
1342-937X/

Our study of the Dalian Basin of North China spanning ca. 1000–920 Ma (Yang et al., 2012; Zhang et al., 2016; Zhao et al., 2019) therefore fills a critical gap in the Tonian $\delta^{13}C$ record and constrains the initiation of Neoproterozoic carbon cycle volatility.

2. Geological setting and studied sections

2.1. Paleogeographic setting

The North China Craton (NCC) was formed by the amalgamation of two blocks between ca. 1.95–1.8 Ga, followed by a long history of deposition from ca. 1.8 Ga to ca. 250 Ma (Zhai and Santosh, 2011; Zhao et al., 2005). Throughout Proterozoic time, the sedimentary depocenter migrated from the southern margin of NCC (the Xiong'er rift system ca. 1.8–1.6 Ga (Cui et al., 2011; Zhao et al., 2002)) to the northern margin of NCC (the Yan-Liao rift system ca. 1.7–1.3 Ga (Gao et al., 2007; Zhang et al., 2015)), and then shifted again to the southeastern NCC margin (the Xuhuai rift system ca. 1.1–0.9 Ga (Peng et al., 2011a; Yang et al., 2012; Zhang et al., 2016)). On the southeastern margin of North China Craton, the ca. 1.1–0.9 Ga Xuhuai rift system covers an area of about 0.1 million km^2 with a maximum extent of about 1000 km and includes the Dalian Basin in the Liaodong Peninsula, the Pyongnam Basin in the central Korean Peninsula, the Xuhuai Basin in the Xuzhou-Huaibei (Xuhuai) area of the Jiangsu and Anhui Provinces, and possibly other basin(s) along the southern margin of NCC (Peng et al., 2011a; Peng et al., 2011b) (Fig. 1). Within each of these basins, there is a Neoproterozoic sequence comprised of clastic sediments at the base and carbonates interlayered with clastic sedimentary rocks at the top.

The Dalian Basin is situated in the southern Liaoning Province (Liaodong Peninsula) of eastern NCC. Before offset of the Tan-Lu (Tanlu) fault took place in the Mesozoic with ~550 km of sinistral displacement (e.g., Xu et al. (1987)), the Dalian Basin was located in the southeastern part of NCC (Fig. 1). The basement of the basin consists of the Archean (ca. 3.8–3.2 Ga) Anshan Complex (e.g., Liu et al., 1992; Wu et al., 2008) and the Paleoproterozoic (ca. 2.2–1.9 Ga) Liaohe Group that were metamorphosed ca. 1.9–1.8 Ga (Li and Zhao, 2007; Zhao et al., 2005). The basement was overlain by the Neoproterozoic and Paleozoic–Cenozoic sedimentary and volcanic rocks (BGMRL, 1989). The Triassic Sulu continent-continent collision resulted in deformation and large scale folding in the region (Yang et al., 2011).

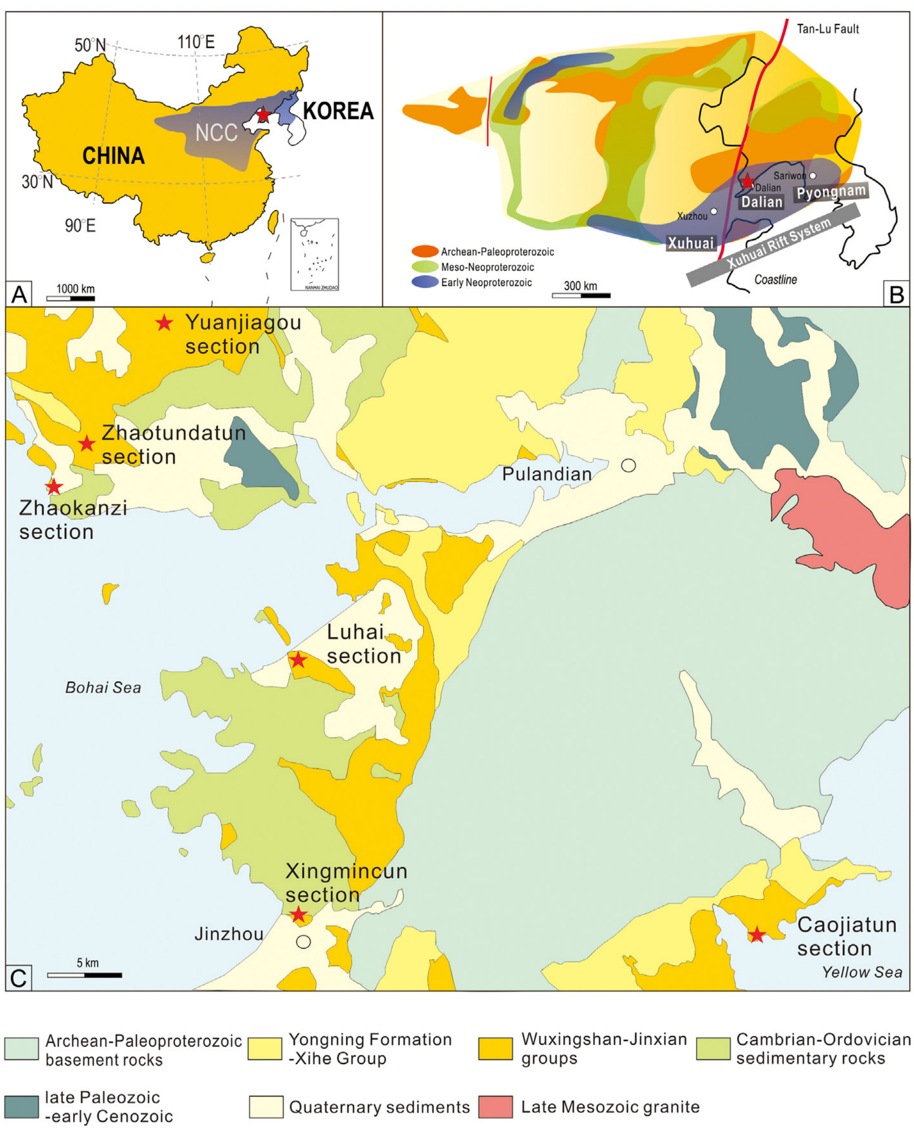

Fig. 1. (A) Geological map of China and Korea Peninsula highlighting North China Craton (NCC, blue). (B) Archean–Paleoproterozoic basement and Mesoproterozoic-Neoproterozoic cover of NCC (modified from Peng et al. (2011a)). (C) Simplified geological map of the early Neoproterozoic sedimentary rocks in the Liaodong Peninsula (Dalian and adjacent region, modified from BGMRL (1989)). Sampled sections are indicated (stars). (For interpretation of the references to colour in this figure legend, the reader is referred to the web version of this article.)

Table 1
Sources of previously published data in Figs. 2 and 7.

Information	Reference
Stratigraphy of the Wuxingshan and Jinxian groups	BGMRL (1989)
Stratigraphy of the Xuhuai Basin	BGMRA (1985)
Stratigraphy of the Pyongnam Basin	Paek et al. (1996)
U-Pb geochronology data	Yang et al., 2012 (1), Zhang et al., 2016 (2), Zhao et al., 2019 (3), Wang et al., 2012 (4), Zhu et al., 2019 (5), He et al., 2017 (6), Sun et al., 2020 (7), Hu et al., 2012 (8), Peng et al., 2011b (9)

2.2. Study sections

The Neoproterozoic strata in the Dalian Basin are composed of three groups (in stratigraphic order): the Xihe, Wuxingshan, and Jinxian groups (BGMRL, 1989) (Fig. 2). The Xihe Group consists of sandstone, shale, and quartzite with some limestone interlayers of the Diaoyu, Nanfen, and Qiaotou formations. The Wuxingshan Group includes (in stratigraphic order) the siliciclastic Changlingzi Formation, the limestone-predominant Nanguanling Formation, and the dolostone-predominant Ganjingzi Formation. The Jinxian Group includes five formations (in stratigraphic order): the carbonate-dominated Yingchengzi, Shisanlitai, and Majiatun formations, the siliciclastic-dominated Cuijiatun Formation, as well as the siliciclastic-carbonate-mixed Xingmincun Formation. The Xihe-Wuxingshan-Jinxian groups uncomformably overlie the Yongning Formation, and are unconformably overlain by the poorly-dated Getun Formation and Dalinzi Formation, which both contain uncorroborated ichnofossils and small shelly fossils (Hong et al., 1991).

Our studied samples were collected from six sections in the Dalian and Jinzhou regions of the Dalian Basin of China (Fig. 1). The Yuanjiagou section (39°29′41.29″N, 121°36′42.85″E) includes the Nanguanling and Ganjingzi formations. The Zhaotundatun section (39°24′06.93″N, 121°31′59.74″E) consists of the Ganjingzi, Yingchengzi (incomplete exposure), and Shisanlitai formations. The Zhaokanzi section (39°23′09.04″N, 121°30′20.67″E) includes the Yingchengzi, Shisanlitai, Majiatun, and Dalinzi (unconformable) formations. The Luhai section (39°17′05.46″N, 121°41′58.64“E) includes the Shisanlitai, Majiatun, Cuijiatun, and Xingmincun formations. The Caojiatun section (39°07′01.65″N, 122°04′18.21″E) includes the Cuijiatun and Xingmincun formations. The Xingmincun section (39°07′35.69″N, 121°42′36.78″E) is composed of the Xingmincun, Getun, and Dalinzi formations. The chemostratigraphy of six sections were spliced together to create a composite $\delta^{13}C$ record using stratigraphic marker beds, lithology, and formational boundaries. Details of the general lithostratigraphy are shown in Fig. 2.

In the Wuxingshan Group, The Nanguanling Formation consists of thin-to-thick-bedded dark gray limestone in the lower part and thick-bedded limestone with interbedded molar tooth structures and stromatolites in the upper part (Fig. 3 A). The succeeding Ganjingzi Formation is up to 300 m in thickness and subdivided into three parts: thick-bedded gray stromatolitic dolostone with calcite dolostone in the lower part, thick-bedded dark gray dolostone in the middle part, and thick-bedded gray dolostone with stromatolitic dolostone in the upper part (Fig. 3 B).

In the Jinxian Group, The Yingchengzi Formation is separated from the underlying Ganjingzi Formation by micritic limestone. The ~110-m-thick Yingchengzi Formation consists of thick-bedded gray micritic and stromatolitic limestone in the lower part and silty limestone in the upper part (Fig. 3 D). The Shisanlitai Formation is ~100 m thick and marked by a red-colored sequence that consists of stromatolitic limestone interbedded with salt and gypsum pseudomorphs in the upper part of the Shisanlitai Formation (Fig. 3E-F). The lower part of the Shisanlitai

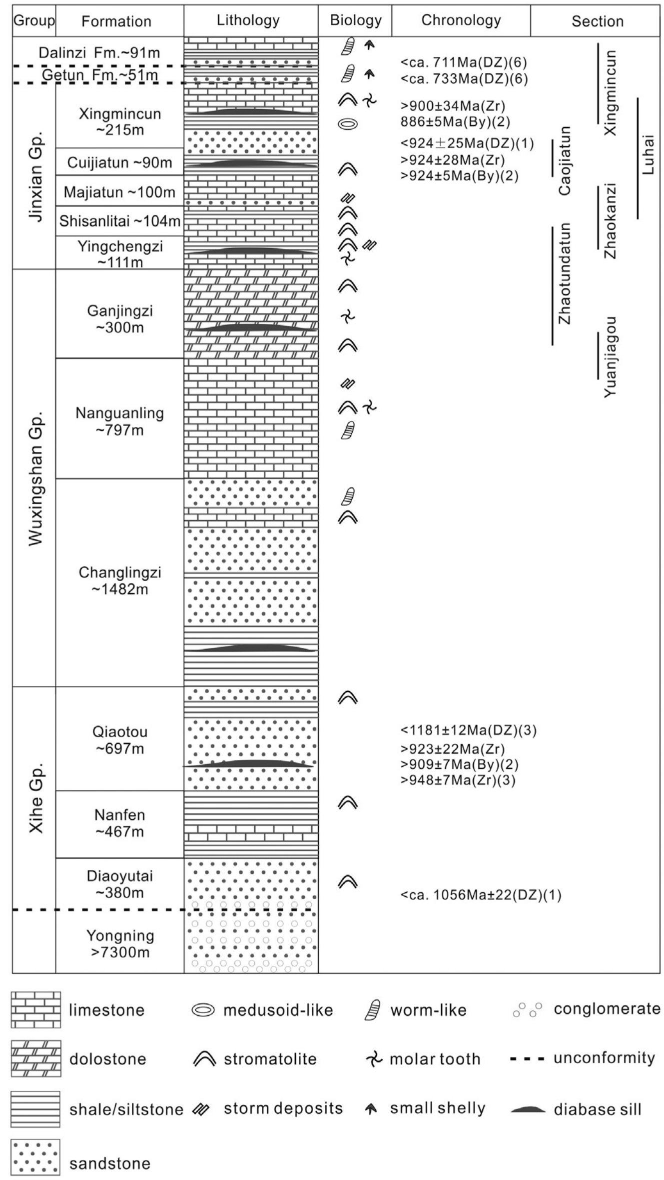

Fig. 2. Simplified stratigraphic column of the Neoproterozoic successions in the Dalian Basin (modified from BGMRL (1989)) with six studied sections shown in Fig. 1. U-Pb geochronologic and biological data are indicated next to the stratigraphic columns. The biology and sedimentary structure information are from: Hong et al. (1991); Kuang et al. (2011); Meng et al. (2006). See Table 1 for sources of previously published lithostratigraphic and geochronological data (detrital zircon in blue; diabase sill in red). By-baddeleyite; DZ-detrital zircon; Zr-magmatic zircon. (For interpretation of the references to colour in this figure legend, the reader is referred to the web version of this article.)

Formation is thick-bedded dark gray stromatolitic limestone (Fig. 3 E). In the Majiatun Formation, the predominant lithology is reddish and light-gray laminar ribbonite limestone (Fig. 3 G-H), and there is an underlying ~1–2-m-thick fine-grained sandstone bed and a ~2–3-m-thick storm-related limestone bed at the base (Fig. 4). The Cuijiatun Formation, ~80 m thick at the Caojiatun section, is dominated by gray silty shale interbedded with columnar stromatolite in the lower part and gray silty shale interbedded with glauconitic-quartz sandstone in the upper part (Fig. 3 I–K). The Xingmincun Formation can be as much as ~215 m in thickness and consists of glauconite-bearing clastic rocks in the lower part, yellowish-green shale in the middle part, and dark gray thin-to-medium-bedded micritic limestone in the upper part (Fig. 3 L–N). Medusoid fossils have been reported in the shale beds of the Xingmincun Formation (Hong et al., 1988; Luo et al., 2016).

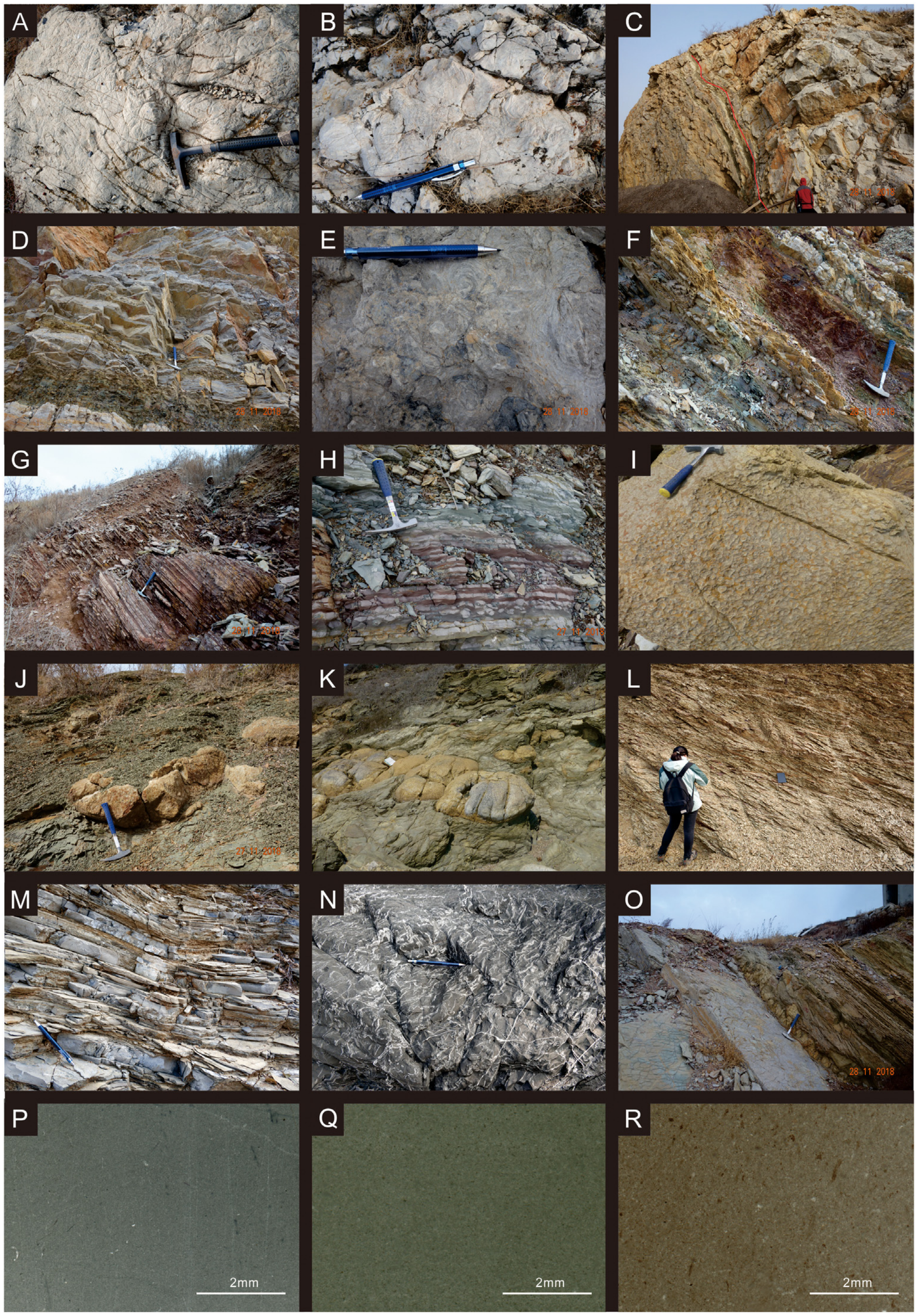

Fig. 3. Field photographs of the Neoproterozoic sedimentary rocks in the Dalian Basin and photomicrographs of carbonate rocks of the Majiatun Formation within the negative carbon isotope excursions of the Zhaokanzi and Luhai sections. A, Dolomitic limestone of the upper Nanguanling Formation, Yuanjiagou section. B, Dolostone with stromatolites of medium thickness in the Ganjingzi Formation. C–D, Boundary between gray limestone layer of medium thickness with shales of the Yingchengzi Formation (D) and thick layers of stromatolites in the Shisanlitai Formation, Zhaokanzi section. E–F, Purple-red and gray stromatolitic limestone (E) with intercalation of yellow-green and purple-red shales (F) in the Shisanlitai Formation, Zhaokanzi section. G–H, Ribbonite limestone in the Majiatun Formation, Zhaokanzi section (G) and Luhai section (H). I–K, Morphological features of stromatolites interlayered in gray-green shale of the Cuijiatun Formation, Luhai section (I, J) and Caojiatun section (K). L–N, Laminar yellow shale in the middle part (L), gray limestone of thin-to-medium thickness in the upper part (M) of the Xingmincun Formation, Luhai section, and molar tooth structures (N) in the Xingmincun Formation, Jinshitan region. O, Unconformity between the underlying carbonate of the Majiatun Formation and the overlying shale of the Dalinzi Formation in the Zhaokanzi section. P–R, Photomicrographs of typical limestone in the Majiatun Formation. (For interpretation of the references to colour in this figure legend, the reader is referred to the web version of this article.)

2.3. Age controls

U-Pb geochronology constrains the Xihe-Wuxingshan-Jinxian Groups of the Dalian Basin to have been deposited ca. 1050–924 Ma: the minimum depositional age of the sequence is constrained by the age of mafic sills (ca. 900 Ma; U-Pb on baddeleyite) (Zhang et al., 2016) intruding the uppermost formation; the maximum depositional age of the uppermost carbonate strata is constrained by the youngest detrital zircon (ca. 924 ± 25 Ma) (Yang et al., 2012); and the maximum depositional age of the sequence is constrained by the youngest detrital

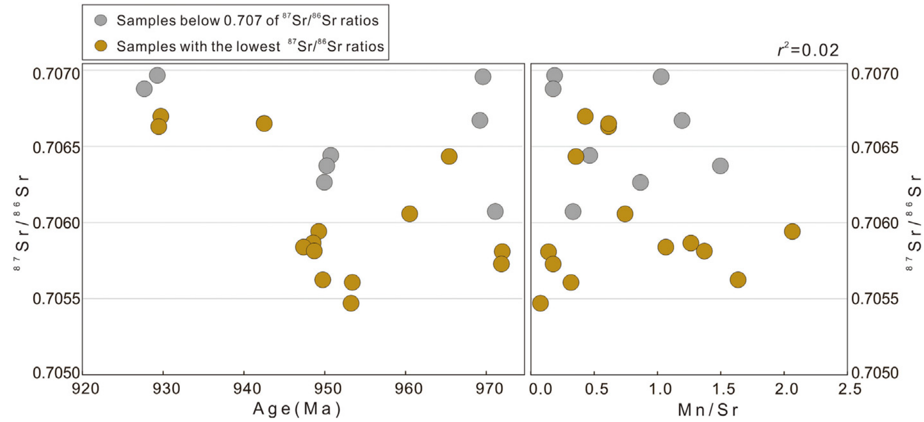

Fig. 4. Measured $^{87}Sr/^{86}Sr$ values for samples of the Wuxingshan and Jinxian groups (left) and a cross-plot of $^{87}Sr/^{86}Sr$ and Mn/Sr (right).

zircon (ca. 1056 ± 22 Ma) from the underlying Diaoyutai Formation (Yang et al., 2012) (Fig. 2). The Xihe-Wuxingshan-Jinxian Groups thus fill a critical gap in the Tonian $\delta^{13}C$ record.

3. Samples and methods

In total, 162 samples from carbonate rocks were collected for stable isotope study from the six sections (Fig. 2). Samples of fresh carbonate were selected, i.e., those without late-stage cements, significant recrystallization, or vein intrusions. Petrographic images of the Majiatun Formation and surrounding units depict compositions of homogenous micritic limestone (>70% carbonate content) with little to no post-depositional alteration (Fig. 3 P–Q). For the element and isotope analyses, 10–20 g of sample fragments were rinsed 3 times with Milli-Q (MQ) water to remove clay minerals and any soluble salts. After drying, the samples were powdered into homogenized powders (~200 meshes) with either a microdrill or an agate mortar.

3.1. Carbon and oxygen stable isotopes

Carbon and oxygen isotope analyses of bulk carbonate samples were performed using a mass spectrometer (MAT 253 (Thermo Fisher Scientific)) with GasBench II system at Institute of Geology and Geophysics, Chinese Academy of Sciences (IGGCAS). Approximately 300 μg of

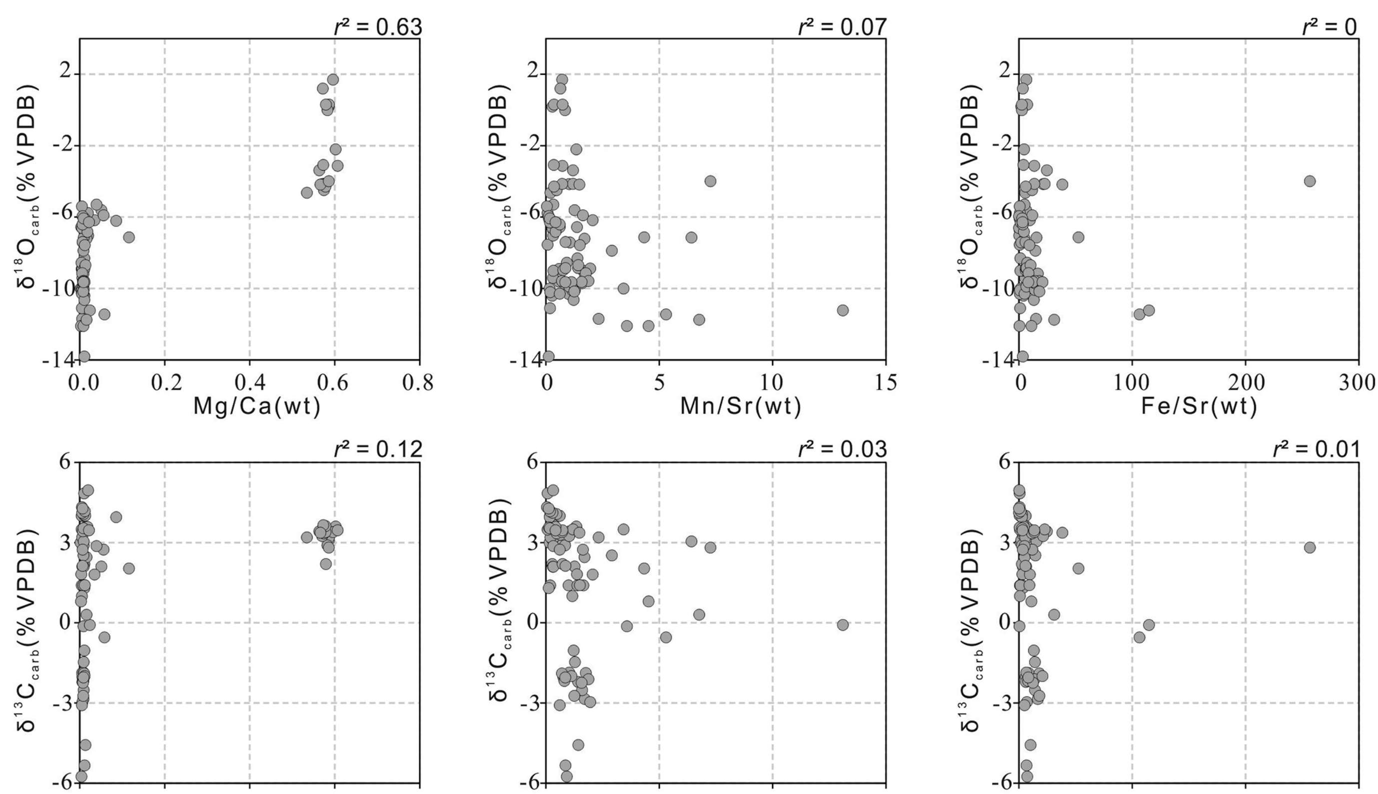

Fig. 5. Cross-plots of geochemical measurements for the Wuxingshan and Jinxian groups. Cross-plots of $\delta^{13}C$ (‰ VPDB) and $\delta^{18}O$ (‰ VPDB) against elemental ratios (Mn/Sr, Fe/Sr, Mg/Ca) are used to evaluate diagenetic alteration and the lithologic dependence of isotopic values. Correlation coefficients of linear regressions (r^2 values) are indicated.

sample powder was reacted with 100% phosphoric acid at 70 °C within a 12 mL vial tube filled with He, and generated CO_2 gas was introduced into the mass spectrometer for measurement of isotopic composition. Precision and accuracy are monitored by running the NBS-19 standard. Isotopic data are expressed in units per mil (‰) relative to Vienna Pee Dee Belemnite (VPDB), and $\delta^{13}C$ and $\delta^{18}O$ were acquired simultaneously. All samples are measured relative to an internal gas standard, and then converted to the VPDB scale using the known composition of NBS-19 ($\delta^{13}C = 1.95$‰; $\delta^{18}O = -2.20$‰) following the correction method of Paul et al. (2007). The reproducibility of the measurements of the standard ($n = 27$) was 0.1‰ (1 σ) for $\delta^{13}C$, and 0.2‰ (1 σ) for $\delta^{18}O$.

3.2. Strontium isotopes

For Sr isotopic analysis, two simple principles were applied for elemental screening: low Mn/Sr mass ratio (in most cases ≤0.8) and high Sr concentration (in most cases, ≥300 μg/g for limestone and ≥ 80 μg/g for dolostone). The dissolution method for strontium isotope is according to Li et al. (2020). Firstly, approximately 100 mg of carbonate rock materials were first pre-leached with 4 mL of 1% acetic acid and ultra-pure water in order to remove the absorbed Sr contamination on mineral surfaces and from ion-exchange sites and clay minerals (Li et al., 2020). Then removing the supernatant, the remained samples were then dissolved in 3.0 mL of 1% acetic acid, and the leachate was dried and re-dissolved in 1.1 mL 2.5 M HCl and finally purified by a resin column filled with 2 mL of AG50W × 12 (200–400 mesh). The Sr isotopic measurements were performed on a Triton Plus TIMS at IGGCAS using a double Re filament. The whole procedure blank was lower than 200 pg for Sr. The mass fractionation of Sr was corrected using an exponential law with $^{88}Sr/^{86}Sr = 8.375209$. The international standard sample NBS-987 was employed to evaluate instrument stability during the period of data collection. Repeated measurement of NBS987 yielded $^{87}Sr/^{86}Sr = 0.710254 \pm 0.000011$ (2σ, $n = 6$, 2SD), showing good agreement with the reported values (Li et al., 2015; Li et al., 2016).

3.3. Element concentrations

For major element analysis, ~50 mg rinsed dry powders were weighed and dissolved with 0.2 M HCl and then diluted before analysis. The element ratios of Mg/Ca, Mn/Sr, and Fe/Sr were analyzed using an IRIS Advantage Inductively Coupled Plasma Optical Emission Spectrometer (ICP-OES) at IGGCAS. A certified reference material was measured after every 10 samples and analytical precision was <3% for analyzed elements.

4. Results

4.1. Carbon and oxygen isotopes

The composite $\delta^{13}C$ record of the six sections is presented in Fig. 7 and the carbon isotope results are provided in Supplementary Table. Consistent $\delta^{13}C$ values and patterns are observed between similar lithologic units from different sections. In the composite isotope stratigraphy, most of the stratigraphy yields slightly positive $\delta^{13}C$ values, but in the Majiatun Formation $\delta^{13}C$ values plunge sharply negative to at far as −5.7‰. This negative excursion in the Majiatun Formation is reproduced in two stratigraphic sections (Luhai and Zhaokanzi). The $\delta^{18}O$ values are variable from −15‰ to 0‰. Generally, tendencies through the stratigraphy have $\delta^{18}O$ increasing to its maximum value (~0‰) in the Ganjingzi Formation, reaching its lowest value (−15‰) in the Cuijiatun Formation, and then returning back to typical values (~ −6‰ to ~ −10‰) in the Xingmincun Formation.

4.2. Strontium isotopes and element concentrations

Strontium isotope compositions and element ratios are shown in Fig. 4 and Supplementary Table. Mn/Sr and Fe/Sr ratios vary from 0.05 to 13.10 and from 0.2 to 256.7, respectively. Mn/Sr ratios are generally below 8.0, with only one exception (13.1). Except two limestone samples in shale layers from the Cuijiatun Formation (106.5 and 114.7), one dolomitic limestone sample from the Nanguanling Formation (256.7), and one sample from the Shisanlitai Formation (52.7), Fe/Sr ratios are between 0.2 and 38.4. Samples display $^{87}Sr/^{86}Sr$ ratios between 0.7055 and 0.7288. The lowest bulk sample $^{87}Sr/^{86}Sr$ ratios from the best-preserved samples, based on the screening methods described above, define ranges of 0.7057–0.7058 in the Nanguanling Formation, 0.7061–0.7064 for dolostone in the Ganjingzi Formation, 0.7055–0.7060 in the Yingchengzi-Shisanlitai formations, and 0.7066–0.7067 in the Majiatun-Xingmincun formations, with Mn/Sr ratios of 0–2.0.

5. Discussion

5.1. Diagenetic alteration

Carbon isotopic composition can be potentially altered by later geological processes (metamorphic materials, siliciclastic grains, authigenic components, burial diagenesis, and/or meteoric diagenesis), especially in Precambrian strata with long and complicated geological histories (Derry, 2010; Kaufman and Knoll, 1995; Knauth and Kennedy, 2009; Schrag et al., 2013). The empirical element concentrations and isotope ratios can be used to identify the magnitude of diagenesis effects, e.g., Mn/Sr, Mg/Ca, Fe/Sr, and $\delta^{18}O/\delta^{13}C$ (Banner, 1995; Brand and Veizer, 1980; Kaufman and Knoll, 1995). Enrichment in Fe and Mn and depletion in Sr for sedimentary carbonates are usually considered to be altered by post-depositional diagenesis (Brand and Veizer, 1980; Derry et al., 1992; Narbonne et al., 1994). Meteoric diagenesis can result in lowering $\delta^{13}C$ or $\delta^{18}O$ values, increasing the Mn/Sr (or Fe/Sr) ratio(s),

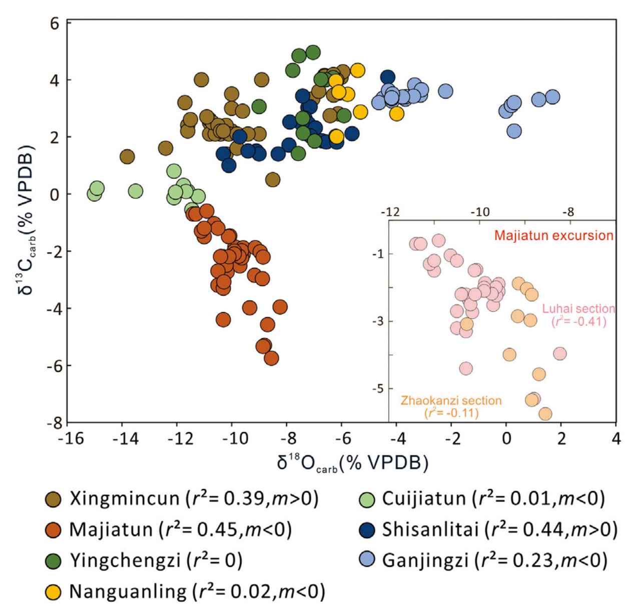

Fig. 6. Cross-plots of $\delta^{18}O$ (‰ VPDB) against $\delta^{13}C$ (‰ VPDB) data for carbonates of the Wuxingshan-Jinxian groups. These m values mean slopes. Linear regression of all data shown yields weakly positive correlations in the Xingmincun (r^2 value = 0.39) and Shisanlitai (r^2 value = 0.44) formations, and weakly negative correlations in the Cuijiatun (r^2 value = 0.01), Majiatun (r^2 value = 0.45), Yingchengzi (r^2 value = 0), Ganjingzi, (r^2 value = 0.23) and Nanguanling (r^2 value = 0.02), arguing against alteration as an explanation of isotopic variations. Inset shows an enlarged view of the Majiatun excursion, and their correlations are both weak and negative in the Luhai section (r^2 value = −0.41) and Zhaokanzi section (r^2 value = −0.11).

and a strong linear correlation between these element and isotope values (Kaufman and Knoll, 1995). Samples with a Mn/Sr ratio < 10 and a Fe/Sr ratio < 40 generally indicate minimal diagenetic alteration of $\delta^{13}C$ signatures (Kaufman and Knoll, 1995; Veizer, 1983). In the Dalian Basin, most samples are characterized by Mn/Sr < 8 and Fe/Sr < 38 (Fig. 5). Cross-correlations between element ratios (Mn/Sr or Fe/Sr) and isotopic ratios ($\delta^{13}C$ or $\delta^{18}O$) are statistically weak (r^2 values << 0.6; Fig. 5). Only one plot ($\delta^{18}O$ vs. Mg/Ca) yields a significant r^2 value (0.63), as the $\delta^{18}O$ values of dolomite are obviously greater than those of calcite (Fig. 5), which show good agreement with isotopic fractionation between these two minerals (Zheng, 2011). Such element ratios and weak cross-correlations indicate our samples only experienced a minor degree of diagenetic alteration and can thus be taken to represent the composition of contemporaneous seawater.

Cross-plotting of $\delta^{13}C$ and $\delta^{18}O$ is also a useful test of diagenesis. Oxygen isotope compositions are sensitive to diagenesis owing to the high concentration of oxygen in diagenetic fluids, whereas carbon isotopic abundances commonly have relatively little influence by meteoric or hydrothermal fluids (Banner and Hanson, 1990; Kaufman and Knoll, 1995). In the studied samples, except for several samples in the Cuijiatun and Xingmincun formations dropping below even −11.5‰, most obtained $\delta^{18}O$ values range from 0‰ to −11.5‰ (Supplementary Table). Meteoric fluids containing dissolved inorganic carbon from oxidized organic matter can lead to decreases in $\delta^{13}C_{carb}$ as well as $\delta^{18}O_{carb}$, yielding a corresponding positive covariation between the two values (Knauth and Kennedy, 2009). A lack of $\delta^{13}C$ and $\delta^{18}O$ covariation in studied successions (r^2 values <0.6) further indicates reliable carbon isotopic compositions of depositional seawater in the Wuxingshan and Jinxian groups (Fig. 6). It is also noteworthy that the C-O correlations in the Majiatun excursion are both weak and negative in the Luhai (r^2 value = 0.41) and Zhaokanzi (r^2 value = 0.11) sections (Fig. 6). The $\delta^{13}C$ excursion in the Majiatun Formation and data from other formations can exclude the possibility of diagenetic alteration and be interpreted as a primary oceanographic signal. We refer to this carbon isotope excursion, for the purposes of this paper, as the Majiatun anomaly, which is reproduced in two stratigraphic sections (Luhai and Zhaokanzi) (Fig. 7) and is consistent with limited previous data from the Majiatun Formation (Hua and Cao, 2004; Qiao et al., 1996).

5.2. Carbon isotope correlation across North China Craton and age calibration of the Majiatun anomaly

Previously published carbon isotope data from the Pyongnam Basin (North Korea) and the Xuhuai Basin (Jiangsu-Anhui Provinces), also from the North China Craton, can similarly be correlated and compared using sequence stratigraphy, paleontology, and intruding sills (Cao, 2000; Hong et al., 1991; Hong and Yang, 1992; Liu et al., 2005; Niu and Zhu, 2002; Peng et al., 2011a; Peng et al., 2011b; Tang et al., 2005; Yin et al., 2015; Zhang et al., 2010). This mid-amplitude excursion (~9‰) to values as negative as ~−6‰ has also been noticed in preliminary $\delta^{13}C$ profiles from these correlative strata across the North China Craton (Fig. 7). In the Xuhuai Basin, $\delta^{13}C$ variations shift from muted

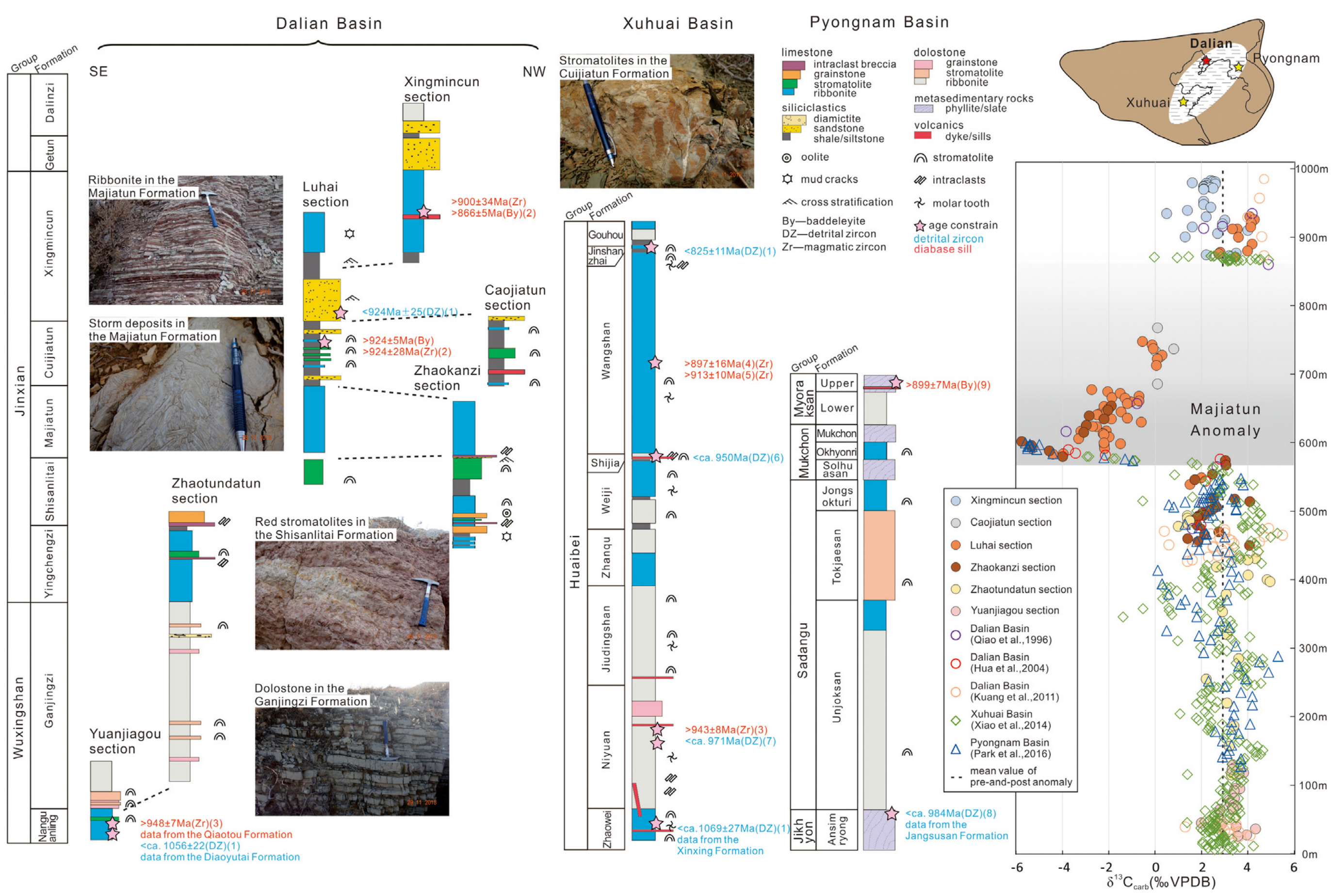

Fig. 7. Composite early Tonian carbon isotope record of the North China Craton (right) and simplified stratigraphic sections through the Dalian-Xuhuai-Pyongnam basins (right) that are correlated on the basis of lithostratigraphy. Carbon isotope profiles are from the Wuxingshan-Jinxian Groups of Dalian Basin (from this study, Qiao et al. (1996), Hua and Cao (2004), and Kuang et al. (2011)) and inferred correlation between the Huaibei Group (Xuhai Basin, Xiao et al. (2014)) and Sangwon Supergroup (Pyongnam Basin, Park et al. (2016)). See Supplementary Table for isotopic data and Table 1 for sources of previously published lithostratigraphic and geochronological data. In the correlation of these basins into a composite $\delta^{13}C$ record for North China Craton, original stratigraphic height data of the Xuhuai basin were modified by a stretching factor of 0.29 and a shift of +62 m for the Wangshan Formation and by a stretching factor of 0.29 and a shift of −85 m for the Shijia to Zhaowei formations based on Xiao et al. (2014). See more lithologic information of the Dalian basin sequence from Fig. 2.

positive values (+0‰ to +5.3‰) in the Zhaowei-Weiji formations to negative values (~−1‰ to −3‰) in the Shijia Formation, and return back to positive values in the Wangshan Formation (0‰ to +5‰) (Xiao et al., 2014). In the Pyongnam Basin, the Sangwon Supergroup exhibits moderately positive $\delta^{13}C$ values between ~0‰ and +5.3‰, until reaching a nadir of ~−6‰ in the Okhyonri Formation of the Mukchon Group (Park et al., 2016). Identification of the Majiatun anomaly across the craton supports the correlation of these basins as well as the fidelity of the anomaly itself (Fig. 7). $^{87}Sr/^{86}Sr$ ratios we studied from ~0.7055 to ~0.7067 are closer to the original Sr isotopic composition than ratios from Zheng et al. (2004) between ~0.7074 and ~0.7080, and our new Sr data are also compatible with an early Tonian age by correlation with Xuhuai basin (Kuang et al., 2011; Zhou et al., 2020). The Xihe-Wuxingshan-Jinxian groups thus fill a critical gap in the Tonian $\delta^{13}C$ record. Furthermore, correlation across North China allows tighter age constraints for the ca. 940 Ma Majiatun anomaly: <950 Ma (Xuhai Basin) and >924 ± 5 Ma Ma (Dalian Basin) (He et al., 2017; Zhang et al., 2016) (Fig. 7). The relatively well-dated Majiatun anomaly starts developing the picture of the early Tonian carbon cycle (Fig. 8).

5.3. Possible origins of the Majiatun anomaly and Neoproterozoic carbon cycle perturbations

As of yet, the Majiatun anomaly has only been observed in North China and thus it may not be a global oceanographic phenomenon. Local explanations are possibly sufficient. For example, mafic sills intruding both the Qiaotou Formation in the Dalian basin and Niyuan Formation in the Xuhuai basin are 945–940-Myr-old (Zhao et al., 2019), potentially coeval with the Majiatun anomaly. The $\delta^{13}C$ values of ~ −6‰ observed are indeed similar to the values for volcanic emissions (~−6–7‰). Furthermore, the Permian/Triassic extinction and associated ~−5‰ carbon excursion has been suggested to be caused by eruption of the coeval Siberian Traps (Renne et al., 1995). However, numerical modeling of the carbon cycle argues that even the extensive Siberian Traps was volumetrically too small and its associated CO_2 emissions were insufficient to cause the magnitude of the negative carbon excursion (Berner, 2002; Payne and Kump, 2007). Therefore, the possibility that the relatively average-sized mafic sills intruding North China at this time could explain the magnitude of the Majiatun anomaly is deemed unlikely. Another possible source of light carbon could be the oxidation of organic matter and/or petroleum leaks, but the Wuxingshan-Jinxian Groups are poor in organic contents (total organic carbon <0.1%; Supplementary Table). Until the Majiatun anomaly is both (i) identified on another continent and (ii) proven to be synchronous, it is difficult to discern whether it is a local or a global oceanographic phenomenon. Nonetheless, being able to rule out the most likely local explanations, we therefore consider more regional-scale explanations for the carbon isotope excursion.

With the identification of the ca. 940 Ma Majiatun anomaly, a more complete picture of $\delta^{13}C$ variation in earliest Neoproterozoic time emerges and establishes the onset of Neoproterozoic carbon cycle volatility (Fig. 8). Prior to our work, the oldest known negative $\delta^{13}C$ anomaly was the ca. 810 Ma Bitter Springs anomaly (Swanson-Hysell et al., 2015). The Majiatun anomaly is as large as the later Bitter Springs anomaly, but significantly pre-dates it by ~130 Myr. In terms of their senses and magnitudes, the negative shifts of ~9‰ of the Bitter Springs and the Majiatun anomalies are identical. Combined isotopic, paleomagnetic, and stratigraphic data suggest that the Bitter Springs anomaly was associated with rapid shifts in paleolatitude of the continents, where temporarily relocating carbon depocenters out of the tropical weathering belt resulted in reduced organic carbon burial and the observed negative excursion (Maloof et al., 2006; Swanson-Hysell et al., 2012). Face-value interpretation of paleomagnetic data from the Bitter Springs Formation itself is consistent with hypothesized rapid shifts in paleolatitude, however the interpretation of the Australian data is ambiguous (Swanson-Hysell et al., 2012). Nonetheless, paleolatitude shifts

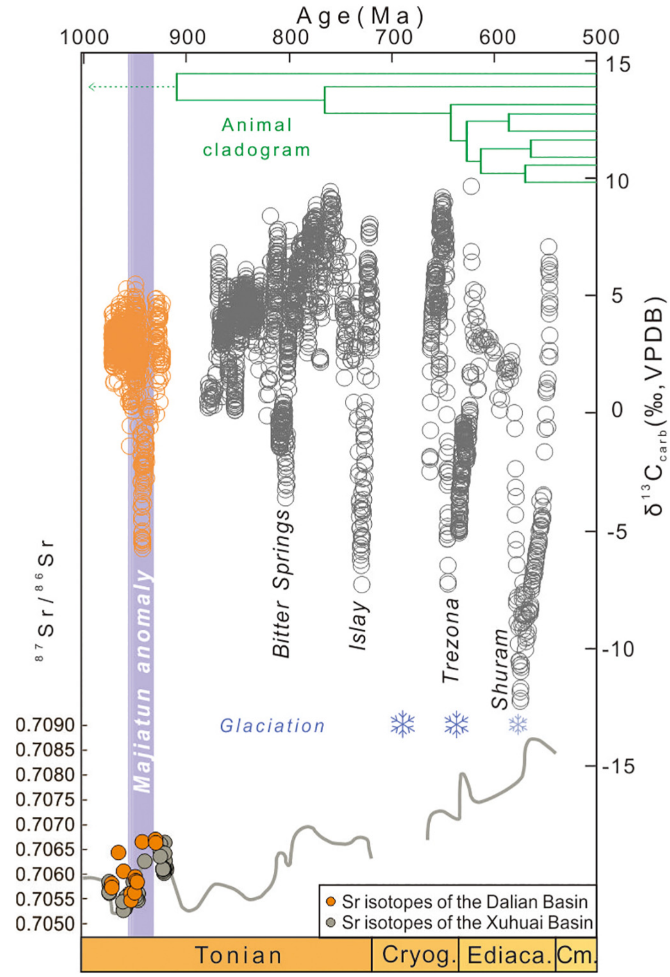

Fig. 8. Carbon and strontium isotopic evolution of Neoproterozoic seawater. New compilation of global carbonate $\delta^{13}C$ from (VPDB—Vienna Peedee belemnite): Neoproterozoic (gray circles; Cox et al. (2016)); early Tonian (orange circles; this study; Supplementary Table). Proposed seawater $^{87}Sr/^{86}Sr$ curve (gray line): Neoproterozoic (gray line; Cox et al. (2016)); early Tonian (orange circles; this study; Supplementary Table). Data compilation Neoproterozoic glaciations are shown as snowflakes: Snowball Earths, big and dark; Gaskiers, small and light). Animal cladogram depicts likely origin of animal multicellularity (Sperling and Stockey, 2018).

during the Bitter Springs anomaly have been documented on multiple continents with high-quality paleomagnetic data (Jing et al., 2020; Maloof et al., 2006; Niu et al., 2016), confirming the link between continental motions and carbon cycle reorganizations (Maloof et al., 2006).

Similar to those observed during the Bitter Springs anomaly, large shifts in the paleolatitude of North China and contiguous continents (Laurentia and Baltica) argues for paleogeographic changes during the Majiatun anomaly (Fairchild et al., 2017; Gong et al., 2018) (Fig. 9). These three continents transited both evaporitic and tropical belts during this time, which would have caused significant changes in weathering and depositional patterns. Motion in/out of the tropics can increase/reduce, respectively, the fraction of organic carbon burial (Maloof et al., 2006). Since these continents were likely part of the larger Rodinia supercontinent at this time (Cawood and Pisarevsky, 2006; Evans, 2009; Li et al., 2008), the changes in continental paleolatitude depicted may be expected globally and therefore of even greater climatic significance. The stratigraphic record of the Dalian Basin is consistent with the departure of the NCC from the tropics during the Majiatun anomaly as stromatolites are abundant and diverse in carbonates both below and above the Majiatun Formation, but absent within it (Hua and Cao, 2004) (Figs. 3 and 7). This observation is consistent with an explanation that a fast shift of paleolatitude may affect the

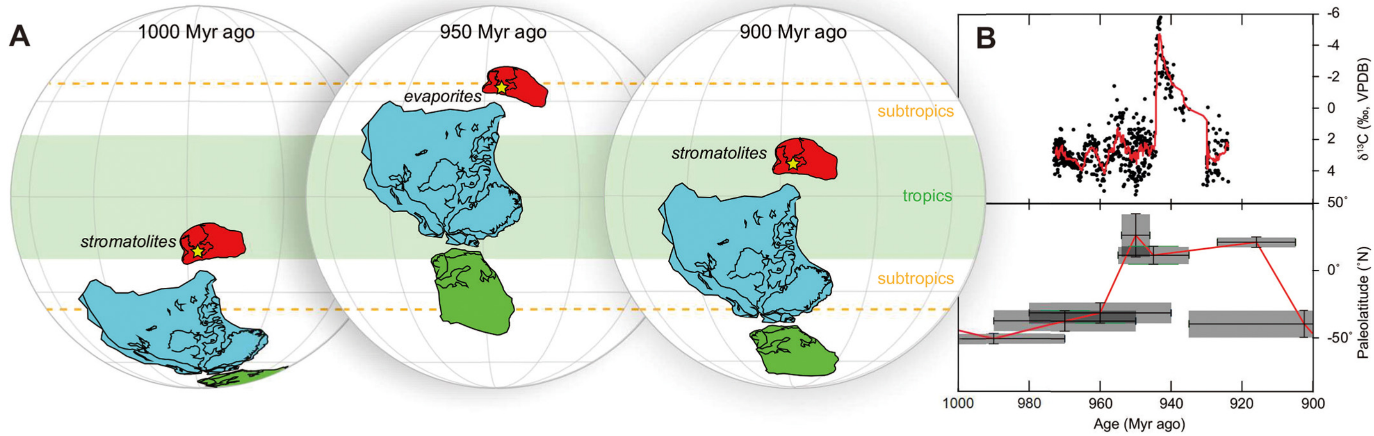

Fig. 9. Paleolatitudinal shifts of continents during the Majiatun anomaly. (A) Paleogeography through time including climatic belts. Green band approximates the tropics, above and below which are the evaporite belts. Continents: Laurentia (blue), Baltica (green), and North China Craton (red), which were part of the larger Rodinia supercontinent. Dalian Basin (indicated by a star). (B) North China Craton composite carbon isotope record (Fig. 7) with 12-point moving average) (top) and paleolatitude of central location (Duluth, MN) during interval (Fairchild et al., 2017) (bottom). Euler rotation parameters for the positions of continents relative to Laurentia in the paleogeographic maps are as follows: Baltica (75.8°, −95.8°, −59.2°) (Li et al., 2008) and North China (50.6°, 19.2°, 56.2°) (Zhao et al., 2019). Then, the paleogeography of Laurentia–Baltica–North China between 1050 Myr ago and 920 Myr ago was reconstructed at the depicted ages using paleomagnetic poles depicted in Fig. 9 B (Fairchild et al., 2017). Note large shifts in continental paleolatitude, and thus weathering and depositional changes, coincide with the Majiatun anomaly. (For interpretation of the references to colour in this figure legend, the reader is referred to the web version of this article.)

numerous environmental conditions (hydrology, light and nutrient availability, sediment inundation, etc.; Corkeron and Slezak, 2020) that control the abundance and diversity of stromatolites. In the red stromatolites of the Shisanlitai Formation, there are elongate gypsum pseudomorphs indicating both high temperature and evaporation (Cao, 2000), consistent with transiting both the tropics and the evaporite belt going into the abrupt anomaly (Fig. 9).

Starting with the Majiatun anomaly, the repeated occurrence of negative Neoproterozoic $\delta^{13}C$ excursions with increasing amplitude over time argues for a protracted prelude leading up the dramatic environmental changes of late Neoproterozoic time including snowball Earth glaciations (Hoffman et al., 2017), ocean-atmosphere oxygenation (Och and Shields-Zhou, 2012), and the innovation of animal multicellularity (Sperling and Stockey, 2018). One leading explanation for the increasingly negative Neoproterozoic carbon isotope excursions is the progressive oxidation of an unusually large oceanic reservoir of organic carbon (Rothman et al., 2003). Atmospheric oxygen levels through the Proterozoic are highly variable rather than stable (Guilbaud et al., 2020). Whether smaller, earlier whiffs of oxygen/oxidant occurred during early Tonian time remains to be resolved. Similar to the Shuram isotope excursion, other extreme negative carbon isotope excursions of the Neoproterozoic are possibly explained by coupled evaporite dissolution and pyrite burial when surplus oxidant is generated through bacterial reduction of sulfate that originates from evaporite weathering (Shields et al., 2019). But since no significant evaporite deposition occurred for hundreds of millions of years prior to the Majiatun anomaly (Evans, 2006), this mechanism may not apply to this earliest-known Neoproterozoic excursion.

Together with other Tonian evolutionary innovations, the abundant occurrence of newly reported multicellular fossils in the Dalian Basin and other Mesoproterozoic and Tonian rocks may have had an impact on oceanic redox structures (Tang et al., 2020). Redox conditions of mid-depth seawater record a shift from predominantly sulfidic to globally ferruginous states in the earliest Neoproterozoic, providing new ecospace for aerobic eukaryotes (Guilbaud et al., 2015). Furthermore, the inferred age between ca. 950–800 Ma for the origin of animal multicellularity from molecular clocks (Sperling and Stockey, 2018) essentially immediately follows the Majiatun anomaly (Fig. 8), suggesting the onset of early Neoproterozoic carbon cycle volatility documented here may be causally related by early animal evolution affecting ocean redox chemistry.

6. Conclusion

An earliest Neoproterozoic carbon isotope anomaly has been documented in the ca. 940 Ma Majiatun Formation of North China. Predating the Bitter Springs anomaly by ~130 Myr, the so-called "Majiatun anomaly" is the first of 5 increasingly negative carbon isotope excursions to occur throughout the era.

Author contributions

Zhiyue Zhang: Investigation; Methodology; Data curation; Visualization; Writing-original draft; Writing - review & editing. Peng Peng: Conceptualization; Funding acquisition; Project administration; Supervision; Investigation; Methodology; Data curation; Validation; Writing-original draft; Writing - review & editing. Lianjun Feng: Methodology; Data curation; Validation; Writing-original draft; Writing - review & editing. Zheng Gong: Methodology; Data curation; Visualization; Writing-original draft; Writing - review & editing. Ross N. Mitchell: Conceptualization; Supervision; Methodology; Data curation; Validation; Visualization; Writing-original draft; Writing - review & editing. Youlian Li: Methodology; Data curation; Writing-original draft.

Declaration of Competing Interest

The authors declare that they have no known competing financial interests or personal relationships that could have appeared to influence the work reported in this paper.

Acknowledgments

The manuscript benefitted from technical support from Xiqiang Zhou, Yanbin Zhang, Hongwei Li, and Yanhong Liu and field support from Xiaotong Zhou, Zhaoyuan Qin, Fengbo Sun, Xinping Wang, and Xiangdong Su. This work was supported by the National Natural Science Foundation of China (41890833, 41772192, 41888101) and Key Research Programs of Chinese Academy of Sciences (IGGCAS-201905, QYZDB-SSWDQC042, GJHZ2016, XDB41000000 and XDB18030205). This is a contribution to IGCP 648.

Appendix A. Supplementary data

Supplementary data to this article can be found online at https://doi.org/10.1016/j.gr.2021.01.013.

References

Banner, J.L., 1995. Application of the trace element and isotope geochemistry of strontium to studies of carbonate diagenesis. Sedimentology 42, 805–824.
Banner, J.L., Hanson, G.N., 1990. Calculation of simultaneous isotopic and trace-element variations during water-rock interaction with applications to carbonate diagenesis. Geochim. Cosmochim. Acta 54, 3123–3137.
Berner, R.A., 2002. Examination of hypotheses for the Permo-Triassic boundary extinction by carbon cycle modeling. Proc. Natl. Acad. Sci. 99, 4172–4177.
Brand, U., Veizer, J., 1980. Chemical diagenesis of a multicomponent carbonate system; 1, Trace elements. J. Sediment. Res. 50, 1219–1236.
Bureau of Geology and Mineral Resources of Anhui (BGMRA), 1985. Strata of Anhui (Precambrian Part). Anhui Sci. and Technology Publishing House, Hefei (174 pp.).
Bureau of Geology and Mineral Resources of Liaoning (BGMRL), 1989. Regional Geology of Liaoning Province. Geology Publishing House, Beijing (856 pp.).
Cao, R., 2000. Discussion on some problems in the Mesoproterozoic and Neoproterozoic stratigraphical study in China. J. Stratigr. 24, 1–7.
Cawood, P.A., Pisarevsky, S.A., 2006. Was Baltica right-way-up or upside-down in the Neoproterozoic? J. Geol. Soc. 163, 753–759.
Corkeron, M., Slezak, P., 2020. Stromatolite framework builders: ecosystems in a Cryogenian interglacial reef. Aust. J. Earth Sci. 67, 833–856.
Cox, G.M., Halverson, G.P., Stevenson, R.K., Vokaty, M., Poirier, A., Kunzmann, M., Li, Z.-X., Denyszyn, S.W., Strauss, J.V., Macdonald, F.A., 2016. Continental flood basalt weathering as a trigger for Neoproterozoic Snowball Earth. Earth Planet. Sci. Lett. 446, 89–99.
Cui, M., Zhang, B., Zhang, L., 2011. U–Pb dating of baddeleyite and zircon from the Shizhaigou diorite in the southern margin of North China Craton: constrains on the timing and tectonic setting of the Paleoproterozoic Xiong'er Group. Gondwana Res. 20, 184–193.
Derry, L.A., 2010. A burial diagenesis origin for the Ediacaran Shuram–Wonoka carbon isotope anomaly. Earth Planet. Sci. Lett. 294, 152–162.
Derry, L.A., Kaufman, A.J., Jacobsen, S.B., 1992. Sedimentary cycling and environmental change in the Late Proterozoic: evidence from stable and radiogenic isotopes. Geochim. Cosmochim. Acta 56, 1317–1329.
Evans, D.A.D., 2006. Proterozoic low orbital obliquity and axial-dipolar geomagnetic field from evaporite palaeolatitudes. Nature 444, 51–55.
Evans, D., 2009. The paleomagnetically viable, long-lived and all-inclusive Rodinia supercontinent reconstruction. Geol. Soc. Lond. Spec. Publ. 327, 371–404.
Fairchild, L.M., Swanson-Hysell, N.L., Ramezani, J., Sprain, C.J., Bowring, S.A., 2017. The end of Midcontinent Rift magmatism and the paleogeography of Laurentia. Lithosphere 9, 117–133.
Gao, L., Zhang, C., Shi, X., Zhou, H., Wang, Z., 2007. Zircon SHRIMP U-Pb dating of the tuff bed in the Xiamaling Formation of the Qingbaikouan System in North China. Geol. Bull. China 26, 249–255.
Gong, Z., Evans, D.A., Elming, S.-Å., Söderlund, U., Salminen, J.M., 2018. Paleomagnetism, magnetic anisotropy and U-Pb baddeleyite geochronology of the early Neoproterozoic Blekinge-Dalarna dolerite dykes, Sweden. Precambrian Res. 317, 14–32.
Grotzinger, J.P., Fike, D.A., Fischer, W.W., 2011. Enigmatic origin of the largest-known carbon isotope excursion in Earth's history. Nat. Geosci. 4, 285–292.
Guilbaud, R., Poulton, S.W., Butterfield, N.J., Zhu, M., Shields-Zhou, G.A., 2015. A global transition to ferruginous conditions in the early Neoproterozoic oceans. Nat. Geosci. 8, 466–U468.
Guilbaud, R., Poulton, S., Thompson, J., Husband, K., Zhu, M., Zhou, Y., Shields-Zhou, G., Lenton, T., 2020. Phosphorus-limited conditions in the early Neoproterozoic ocean maintained low levels of atmospheric oxygen. Nat. Geosci. 13, 296–301.
He, T., Zhou, Y., Vermeesch, P., Rittner, M., Miao, L., Zhu, M., Carter, A., Pogge von Strandmann, P.A.E., Shields, G.A., 2017. Measuring the 'Great Unconformity' on the North China Craton using new detrital zircon age data. Geol. Soc. Lond. Spec. Publ. 448, 145–159.
Hoffman, P.F., Abbot, D.S., Ashkenazy, Y., Benn, D.I., Brocks, J.J., Cohen, P.A., Cox, G.M., Creveling, J.R., Donnadieu, Y., Erwin, D.H., Fairchild, I.J., Ferreira, D., Goodman, J.C., Halverson, G.P., Jansen, M.F., Le Hir, G., Love, G.D., Macdonald, F.A., Maloof, A.C., Partin, C.A., Ramstein, G., Rose, B.E.J., Rose, C.V., Sadler, P.M., Tziperman, E., Voigt, A., Warren, S.G., 2017. Snowball Earth climate dynamics and Cryogenian geology-geobiology. Sci. Adv. 3, e1600983.
Hong, Z., Huang, Z., Yang, X., Lan, J., Xian, B., Yang, Y., Liu, X., 1988. Medusoid fossils from the Sinian Xingmincun Formation of southern Liaoning. Acta Geol. Sin. 62, 200–209.
Hong, Z., Liu, X., Yang, Y., Huang, Z., 1991. Macrofossil sequence of the late Precambrian from the southern Liaodong Peninsula. Land Resour. 3, 219–236.
Hong, Z., Yang, Y., 1992. The stratigraphic correlation of the upper Precambrian of southern Liaoning with that of southern Jilin, Jiangsu Anhui and northern Korea. Region. Geol. China 76–84.
Hu, B., Zhai, M., Li, T., Li, Z., Peng, P., Guo, J., Kusky, T., 2012. Mesoproterozoic magmatic events in the eastern North China Craton and their tectonic implications: Geochronological evidence from detrital zircons in the Shandong Peninsula and North Korea. Gondwana Res. 22 (3–4), 828–842.
Hua, H., Cao, R., 2004. An abrupt variation event of stromatolitic microstructures in the Neoproterozoic and its origination background. Acta Palaeontol. Sin. 43, 234–245.
Jing, X., Yang, Z., Evans, D.A.D., Tong, Y., Xu, Y., Wang, H., 2020. A pan-latitudinal Rodinia in the Tonian true polar wander frame. Earth Planet. Sci. Lett. 530, 115880.
Kaufman, A.J., Knoll, A.H., 1995. Neoproterozoic variations in the C-isotopic composition of seawater: stratigraphic and biogeochemical implications. Precambrian Res. 73, 27–49.
Knauth, L.P., Kennedy, M.J., 2009. The late Precambrian greening of the Earth. Nature 460, 728–732.
Kuang, H., Liu, Y., Peng, N., Liu, L., 2011. Geochemistry of the Neoproterozoic molar-tooth carbonates in Dalian,eastern Liaoning, China, and its geological implications. Earth Sci. Front. 18, 25–40.
Li, S., Zhao, G., 2007. SHRIMP U-Pb zircon geochronology of the Liaoji granitoids: Constraints on the evolution of the paleoproterozoic Jiao-Liao-Ji belt in the eastern block of the North China craton. Precambrian Res. 158, 1–16.
Li, Z.X., Bogdanova, S.V., Collins, A.S., Davidson, A., De Waele, B., Ernst, R.E., Fitzsimons, I.C.W., Fuck, R.A., Gladkochub, D.P., Jacobs, J., Karlstrom, K.E., Lu, S., Natapov, L.M., Pease, V., Pisarevsky, S.A., Thrane, K., Vernikovsky, V., 2008. Assembly, configuration, and break-up history of Rodinia: a synthesis. Precambrian Res. 160, 179–210.
Li, C., Planavsky, N.J., Love, G.D., Reinhard, C.T., Hardisty, D., Feng, L., Bates, S.M., Huang, J., Zhang, Q., Chu, X., Lyons, T.W., 2015. Marine redox conditions in the middle Proterozoic Ocean and isotopic constraints on authigenic carbonate formation: insights from the Chuanlinggou Formation, Yanshan Basin, North China. Geochim. Cosmochim. Acta 150, 90–105.
Li, C., Wang, X., Jinghui, G., Chu, Z., Feng, L.J., 2016. Rapid separation scheme of Sr, Nd, Pb, and Hf from a single rock digest using a tandem chromatography column prior to isotope ratio measurements by mass spectrometry. J. Anal. At. Spec. 31, 1150–1159.
Li, Y., Li, C., Guo, J., 2020. Re-evaluation and optimisation of dissolution methods for strontium isotope stratigraphy based on chemical leaching of carbonate certificated reference materials. Microchem. J. 154, 104607.
Liu, D., Nutman, A., Compston, W., Wu, J., Shen, Q.H., 1992. Remnants of ≥3800 Ma crust in the Chinese part of the Sino-Korean craton. Geology 20, 339–342.
Liu, Y., Kuang, H., Meng, X., Ge, M., Cai, G., 2005. The Neoproterozoic stratigraphic correlation framework in the Jilin-Liaoning-Xuzhou-Huaiyang area. J. Stratigr. 29, 387–396.
Luo, C., Zhu, M., Reitner, J., 2016. The Jinxian Biota revisited: taphonomy and body plan of the Neoproterozoic discoid fossils from the southern Liaodong Peninsula, North China. Paläontol. Z. 90, 205–224.
Lyons, T.W., Reinhard, C.T., Planavsky, N.J., 2014. The rise of oxygen in Earth's early ocean and atmosphere. Nature 506, 307–315.
Macdonald, F.A., Schmitz, M.D., Crowley, J.L., Roots, C.F., Jones, D.S., Maloof, A.C., Strauss, J.V., Cohen, P.A., Johnston, D.T., Schrag, D.P., 2010. Calibrating the Cryogenian. Science 327, 1241–1243.
Maloof, A.C., Halverson, G.P., Kirschvink, J.L., Schrag, D.P., Weiss, B.P., Hoffman, P.F., 2006. Combined paleomagnetic, isotopic, and stratigraphic evidence for true polar wander from the Neoproterozoic Akademikerbreen Group, Svalbard, Norway. Geol. Soc. Am. Bull. 118, 1099–1124.
Meng, X., Ge, M., Liu, Y., 2006. Study of the Neoproterozoic microspar (molar tooth) carbonate events, sequence stratigraphy of the Sino-Korean plate and the establishment of the Beihuan system. J. Stratigr. 30, 21–32.
Narbonne, G.M., Kaufman, A.J., Knoll, A.H., 1994. Integrated chemostratigraphy and biostratigraphy of the Windermere Supergroup, northwestern Canada: implications for Neoproterozoic correlations and the early evolution of animals. Geol. Soc. Am. Bull. 106, 1281–1292.
Niu, S., Zhu, S., 2002. On the Huainan biota. J. Stratigr. 26, 1–8.
Niu, J., Li, Z., Zhu, W., 2016. Palaeomagnetism and geochronology of mid-Neoproterozoic Yanbian dykes, South China: Implications for a c. 820-800 Ma true polar wander event and the reconstruction of Rodinia. Geol. Soc. Lond. Spec. Publ. 424, 191–211.
Och, L.M., Shields-Zhou, G.A., 2012. The Neoproterozoic oxygenation event: environmental perturbations and biogeochemical cycling. Earth Sci. Rev. 110, 26–57.
Paek, R.J., Gap, K.H., Jon, G.P. (Eds.), 1996. Geol. Of Korea. Foreign Languages Books Publishing House, Pyongyang (631 pp.).
Park, H., Zhai, M., Yang, J., Peng, P., Kim, J., Zhang, Y., Kim, M., Park, U., Feng, L., 2016. Deposition age of the sangwon supergroup in the pyongnam Basin (Korea) and the Early Tonian negative carbon isotope interval. Acta Petrol. Sin. 32, 2181–2195.
Paul, D., Skrzypek, G., Fórizs, I., 2007. Normalization of measured stable isotopic compositions to isotope reference scales – a review. Rapid Commun. Mass Spec. 21, 3006–3014.
Payne, J.L., Kump, L.R., 2007. Evidence for recurrent Early Triassic massive volcanism from quantitative interpretation of carbon isotope fluctuations. Earth Planet. Sci. Lett. 256, 264–277.
Peng, P., Bleeker, W., Ernst, R.E., Söderlund, U., Mcnicoll, V., 2011a. U–Pb baddeleyite ages, distribution and geochemistry of 925 Ma mafic dykes and 900 Ma sills in the North China craton: evidence for a Neoproterozoic mantle plume. Lithos 127, 210–221.
Peng, P., Zhai, M.-G., Li, Q., Wu, F., Hou, Q., Li, Z., Li, T., Zhang, Y., 2011b. Neoproterozoic (~900Ma) Sariwon sills in North Korea: geochronology, geochemistry and implications for the evolution of the south-eastern margin of the North China Craton. Gondwana Res. 20, 243–254.
Qiao, X., Song, T., Li, H., Gao, L., 1996. Genetic Stratigraphy of the Sinian and Lower Cambrian Strata in South Liaoning Province. Sci. Press, Beijing.
Renne, P.R., Zhang, Z.C., Richards, M.A., Black, M.T., Basu, A.R., 1995. Synchrony and causal relations between Permian-Triassic boundary crises and Siberian flood volcanism. Science 269, 1413–1416.
Rose, C.V., Swanson-Hysell, N.L., Husson, J.M., Poppick, L.N., Cottle, J.M., Schoene, B., Maloof, A.C., 2012. Constraints on the origin and relative timing of the Trezona delta C-13 anomaly below the end-Cryogenian glaciation. Earth Planet. Sci. Lett. 319, 241–250.

Rothman, D.H., Hayes, J.M., Summons, R.E., 2003. Dynamics of the Neoproterozoic carbon cycle. Proc. Natl. Acad. Sci. 100, 8124–8129.

Schrag, D.P., Higgins, J.A., Macdonald, F.A., Johnston, D.T., 2013. Authigenic carbonate and the history of the global carbon cycle. Science 339, 540–543.

Shields, G.A., Mills, B.J.W., Zhu, M., Raub, T.D., Daines, S.J., Lenton, T.M., 2019. Unique Neoproterozoic carbon isotope excursions sustained by coupled evaporite dissolution and pyrite burial. Nat. Geosci. 12, 823–827.

Sperling, E.A., Stockey, R.G., 2018. The temporal and environmental context of early animal evolution: considering all the ingredients of an "explosion". Integr. Comp. Biol. 58, 605–622.

Sun, F.B., Peng, P., Zhou, X.Q., Magalhaes, A.J.C., Guadagnin, F., Zhou, X.T., Zhang, Z.Y., Su, X.D., 2020. Provenance analysis of the late Mesoproterozoic to early Neoproterozoic Xuhuai Basin in the southeast North China Craton: Implications for paleogeographic reconstruction. Precambrian Res. 337, 105554.

Swanson-Hysell, N.L., Maloof, A.C., Kirschvink, J.L., Evans, D.A.D., Halverson, G.P., Hurtgen, M.T., 2012. Constraints on Neoproterozoic paleogeography and Paleozoic orogenesis from paleomagnetic records of the Bitter Springs Formation, Amadeus Basin, Central Australia. Am. J. Sci. 312, 817–884.

Swanson-Hysell, N.L., Maloof, A.C., Condon, D.J., Jenkin, G.R.T., Alene, M., Tremblay, M.M., Tesema, T., Rooney, A.D., Haileab, B., 2015. Stratigraphy and geochronology of the Tambien Group, Ethiopia: evidence for globally synchronous carbon isotope change in the Neoproterozoic. Geology 43, 323–326.

Tang, F., Yin, C., Wang, Z., Chen, M., 2005. Advances and development trend in the study of the stratigraphic correlation of the Neoproterozoic and megafossils on the eastern margin of the North China platform. Geol. Bull. China 24, 589–596.

Tang, Q., Pang, K., Yuan, X., Xiao, S., 2020. A one-billion-year-old multicellular chlorophyte. Nat. Ecol. Evol. 4, 543–549.

Veizer, J., 1983. Chemical diagenesis of carbonates: theory and application of trace element technique. Stable Isotop. Sediment. Geol. 10, 3.1–3.100.

Wang, Q., Yang, D., Xu, W., 2012. Neoproterozoic basic magmatism in the southeast margin of North China Craton: Evidence from whole-rock geochemistry, U-Pb and Hf isotopic study of zircons from diabase swarms in the Xuzhou-Huaibei area of China. Sci. China Earth Sci. 55, 1461–1479.

Wu, F., Zhang, Y., Yang, J., Xie, L., Yang, Y., 2008. Zircon U–Pb and Hf isotopic constraints on the Early Archean crustal evolution in Anshan of the North China Craton. Precambrian Res. 167, 339–362.

Xiao, S., Shen, B., Tang, Q., Kaufman, A.J., Yuan, X., Li, J., Qian, M., 2014. Biostratigraphic and chemostratigraphic constraints on the age of early Neoproterozoic carbonate successions in North China. Precambrian Res. 246, 208–225.

Xu, J., Zhu, G., Tong, W., Cui, K., Liu, Q., 1987. Formation and evolution of the Tancheng-Lujiang wrench fault system: a major shear system to the northwest of the Pacific Ocean. Tectonophysics 134, 273–310.

Yang, T., Peng, Y., Leech, M., Lin, H., 2011. Fold patterns indicating Triassic constrictional deformation on the Liaodong peninsula, eastern China, and tectonic implications. J. Asia Earth Sci. 40, 72–83.

Yang, D., Xu, W., Xu, Y., Wang, Q., Pei, F., Wang, F., 2012. U–Pb ages and Hf isotope data from detrital zircons in the Neoproterozoic sandstones of northern Jiangsu and southern Liaoning Provinces, China: Implications for the Late Precambrian evolution of the southeastern North China Craton. Precambrian Res. 216-219, 162–176.

Yin, C., Gao, L., Liu, P., Tang, F., Wang, Z., Chen, S., 2015. Neoproterozoic Stratigraphic Sequence and Chronostratigraphic Division in China. Sci. Press.

Zhai, M., Santosh, M., 2011. The early Precambrian odyssey of the North China Craton: a synoptic overview. Gondwana Res. 20, 6–25.

Zhang, L., Zhang, L., Hu, Y., 2010. Constrast and study on forming stage of neoproterozoic and stratigraphic division in Xuzhou Huaihe River Region Jilin Province and Liaoning Province. Shandong Land Resour. 26, 8–12.

Zhang, Y., Li, Q., Lan, Z., Wu, F., Li, X., Yang, J., Zhai, M., 2015. Diagenetic xenotime dating to constrain the initial depositional time of the Yan-Liao Rift. Precambrian Res. 271, 20–32.

Zhang, S., Zhao, Y., Ye, H., Hu, G., 2016. Early Neoproterozoic emplacement of the diabase sill swarms in the Liaodong Peninsula and pre-magmatic uplift of the southeastern North China Craton. Precambrian Res. 272, 203–225.

Zhao, T., Zhou, M., Zhai, M., Xia, B., 2002. Paleoproterozoic rift-related volcanism of the Xiong'er Group, North China craton: implications for the breakup of Columbia. Int. Geol. Rev. 44, 336–351.

Zhao, G., Sun, M., Wilde, S.A., Sanzhong, L., 2005. Late Archean to Paleoproterozoic evolution of the North China Craton: key issues revisited. Precambrian Res. 136, 177–202.

Zhao, H., Zhang, S., Ding, J., Chang, L., Ren, Q., Li, H., Yang, T., Wu, H., 2019. New geochronologic and paleomagnetic results from early Neoproterozoic mafic sills and late Mesoproterozoic to early Neoproterozoic successions in the eastern North China Craton, and implications for the reconstruction of Rodinia. GSA Bull. 132, 739–766.

Zheng, Y., 2011. On the theoretical calculations of oxygen isotope fractionation factors for carbonate-water systems. Geochem. J. 45, 341–354.

Zheng, W., Yang, J., Hong, T., 2004. Sr and C isotopic correlation and the age boundary determination for the Neoproterozoic in the Southern Liaoning and Northern Jiangsu-Northern Anhui Provinces. Geol. J. China Univ. 30, 691–699.

Zhou, Y., Pogge von Strandmann, P.A., Zhu, M., Ling, H., Manning, C., Li, D., He, T., Shields, G.A., 2020. Reconstructing Tonian seawater 87Sr/86Sr using calcite microspar. Geology 48, 462–467.

Zhu, R.Z., Ni, P., Wang, G.G., Ding, J.Y., Fan, M.S., Ma, Y.G., 2019. Geochronology, geochemistry and petrogenesis of the Laozhaishan dolerite sills in the southeastern margin of the North China Craton and their geological implication. Gondwana Res. 67, 131–146.